The fabrication and the coercivity mechanism of segmented $(Ni/Fe)_m$ composite nanowire arrays

2004 J. Phys.: Condens. Matter 16 8775

(http://iopscience.iop.org/0953-8984/16/47/027)

INSTITUTE OF PHYSICS PUBLISHING JOURNAL OF PHYSICS: CONDENSED MATTER

J. Phys.: Condens. Matter **16** (2004) 8775–8782 PII: S0953-8984(04)80688-X

The fabrication and the coercivity mechanism of segmented $(Ni/Fe)_m$ composite nanowire arrays

D S Xue, H G Shi[1] and M S Si

Key Laboratory of Magnetism and Magnetic Materials of the Ministry of Education, Lanzhou University, Lanzhou 730000, People's Republic of China

E-mail: shihuig@lzu.edu.cn

Received 9 May 2004, in final form 25 October 2004
Published 12 November 2004
Online at stacks.iop.org/JPhysCM/16/8775
doi:10.1088/0953-8984/16/47/027

Abstract

Arrays of segmented $(Ni/Fe)_m$ ($m = 1, 2, 3, 4, 5$) composite nanowires about 3 μm in length and with aspect ratios of about 60 were electrodeposited on anodic porous alumina templates using a dual bath. The structure, morphology and magnetic properties of the samples were characterized by means of x-ray diffraction, transmission electron microscopy and vibrating sample magnetometry, respectively. It is found that Fe(110) and Ni(111) orientations along nanowire axis are preferred. The large aspect ratio of the composite nanowires reveals a strong shape magnetic anisotropy. As the number of the Ni/Fe composite segments m increases, the coercivity of the nanowire arrays, with the magnetic field applied parallel to the wire, gradually increases. The coercivity variation of the segmented composite nanowires is closely related to the effective exchange coupling between the Ni and Fe segments.

1. Introduction

Exchange interaction plays an important role in the spontaneous magnetization of magnetic materials. However, the exchange coupling affects the magnetization reversal process due to the change of the different magnetic phase layer thicknesses in the trilayers, so the coercivity can be changed [1]. In recent years, much attention has been focused on research into and achieving an understanding of magnetic exchange coupling in nanocomposites that are composed of magnetically different magnetic phases [2]. Such composite systems are promising as regards advanced magnetic applications. At the same time, the magnetic nanowire arrays are of great interest for both their fundamental science and potential applications in, e.g., high density perpendicular magnetic recording media and nanosensors [3–5]. Recently, Skomski *et al* studied the magnetization reversal in the single metals Fe, Co and

[1] Author to whom any correspondence should be addressed.

0953-8984/04/478775+08$30.00

Ni and their alloys [6–8]. However, few works on magnetization reversal in segmented composite nanowire arrays have been reported. If the coercivity can be adjusted by changing the exchange coupling in segmented composite nanowire arrays, this is very important for technical applications.

Generally, the nanowire arrays exhibiting both high coercivity and shape magnetic anisotropy have high aspect ratios. It is know that the chain-of-spheres model with a fanning mechanism describes the behaviour of elongated single-domain particles well [9, 10]. Almawlawai *et al* [11] and Zhan *et al* [12] demonstrated that the symmetric fanning mechanism of the sphere–chain model is a good model for magnetization reversal, at least when the applied field lies along the single-metal or alloy wire axis. If segmented $(Ni/Fe)_m$ composite nanowires with the same length and diameter are fabricated, the m dependence of the coercivity can be affected due to the contribution of the effective exchange coupling between the Fe and Ni segments.

Among the methods of fabricating arrays of nanowires, self-ordered anodized aluminium oxide (AAO) template synthesis by electrodeposition has proved to be a particularly high yield technique for preparing arrays of nanowires [13–15]. There are two approaches for fabricating arrays of segmented metal composite nanowires by electrodeposition. In most of the experimental work, a single-bath technique using an electrolyte solution containing two or more different metal ions is used, which causes co-deposition of the different metal ions. It is difficult to get a highly pure composition in each segment. An alternative approach is the dual-bath technique in which the substrate is moved between two different electrolyte baths [16, 17]. Consequently, co-deposition of the different metal ions can be avoided. Herein, we report fabrication using the dual-bath technique and the coercivity variation for arrays of segmented $(Ni/Fe)_m$ composite nanowires.

2. Experiments

An ordered AAO template was fabricated using a superpurity Al sheet (99.99%). The aluminium sheet was degreased ultrasonically in absolute ethyl alcohol for approximately 15 min, etched in 1.0 M NaOH at room temperature for 15 min to remove the native oxide and washed thoroughly with distilled water, then electropolished in a mixed solution of $HClO_4$:CH_3CH_2OH = 1:4 for 2 min and immediately rinsed with distilled water. Afterwards, the Al sheet was anodized at 40 V_{DC} in 0.3 M $H_2C_2O_4$ aqueous solution at 11 °C using a two-step anodizing method [18].

Using the dual-bath technique, Ni and Fe segments were alternately electrodeposited into the pores for the same time by moving the substrate between two different electrolyte baths. One bath consisted of $NiSO_4{\cdot}6H_2O$ (120 g l^{-1}) and boric acid (45 g l^{-1}). The other consisted of $FeSO_4{\cdot}7H_2O$ (120 g l^{-1}), boric acid (45 g l^{-1}) and ascorbic acid (1 g l^{-1}). The deposition of the segments was carried out at room temperature with a graphite counter-electrode. The total deposition time remained constant for 4 min. 100 and 200 Hz currents were used to deposit Ni and Fe segments, respectively, at 13 V_{AC}. Five samples each about 3 μm in length were fabricated by shortening the deposition time for each segment with increasing number of segments.

The phase structure of these composite nanowires was characterized by means of x-ray diffraction (XRD) using an X'Pert PRO diffractometer from Philips with Cu Kα radiation. The morphology was obtained by JEM-1200EX transmission electron microscopy (TEM) after having completely dissolved the AAO in 1.0 M NaOH aqueous solution. The magnetization measurement was performed at room temperature employing a VSM7304-type vibrating sample magnetometer (VSM) from Lakeshore.

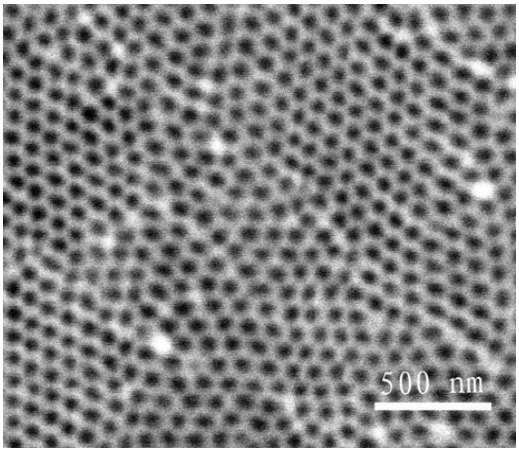

Figure 1. An SEM image of the AAO template.

3. Results and discussion

The quality and distribution of the pore sizes in the template play an important role in forming nanowires and in measuring magnetic properties. Figure 1 shows a representative SEM image of the AAO template obtained with a two-step anodizing process in 0.3 M $H_2C_2O_4$ aqueous solution. Clearly, the shape of the pores is approximately hexagonal; the average diameter and the space between the pores are both about 50 nm. The pore channels in the AAO films are uniform, parallel to each other and perpendicular to the membrane surface [14].

Figure 2 shows representative XRD patterns of the segmented $(Ni/Fe)_m$ composite nanowires. It is found that each pattern is composed of a background smoothly increasing with decreasing diffraction angle and seven sharp peaks. The former arises from the AAO template and the latter from the diffractions of the coexisting Ni and Fe phases. The sharp peaks of the (110), (200), (211), (220) diffractions indicate that the Fe segment has a bcc structure. The sharp peaks of the (111), (200), (220), (311) diffractions peaks show that the Ni segment has a fcc structure. It is significant that both the Fe(110) and Ni(111) diffraction peaks have preferred orientation along the wire axes. However, because of the overlap of the Fe(110) and Ni(111) diffraction peaks, it is difficult to determine the degrees of orientation for the two phases.

Figure 3 shows a TEM micrograph of the segmented $(Ni/Fe)_m$ composite nanowires. Clearly, the nanowires are regular and uniform with diameter about 50 nm, length about 3 μm and aspect ratio (length divided by diameter) about 60. The diameter is consistent with the SEM image of the AAO template. The length is in approximate agreement with the deposition rates of Ni (approximately 500 nm min^{-1}) and Fe (approximately 1000 nm min^{-1}).

The representative hysteresis loops measured at room temperature by the VSM are shown in figure 4. It is found that when the applied field is parallel ($H_\parallel$) and perpendicular ($H_\perp$) to the wire axis, the ratios of remanence to saturation magnetization are about 0.83 and 0.06, and the coercivities H_c have magnitudes of about 1500 and 400 Oe. This indicates that the high magnetic anisotropy results from the preferred orientation along the wire axis. It is noted that the hysteresis loop is a smooth and simple loop with no evidence for two H_c values for Ni and Fe segments. This indicates that there is an effective exchange coupling between Ni and Fe segments.

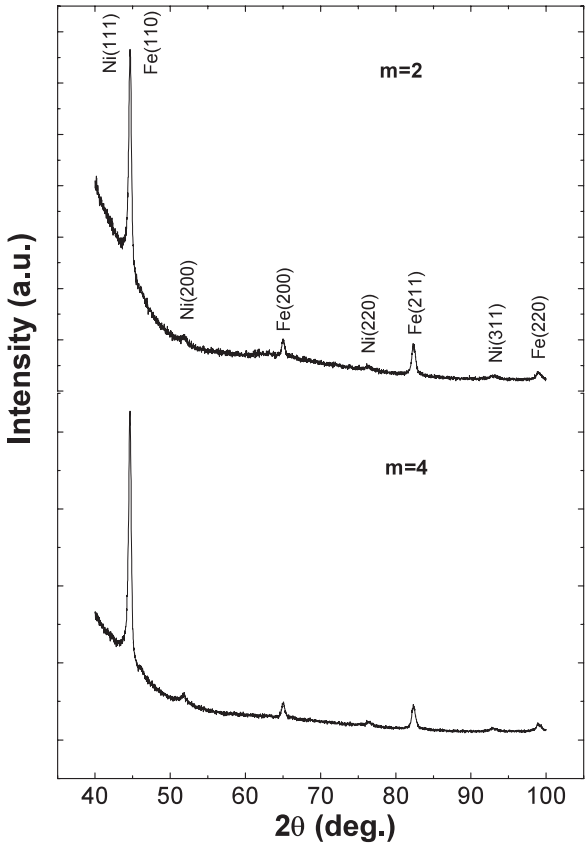

Figure 2. X-ray diffraction patterns of the segmented $(Ni/Fe)_m$ composite nanowire arrays.

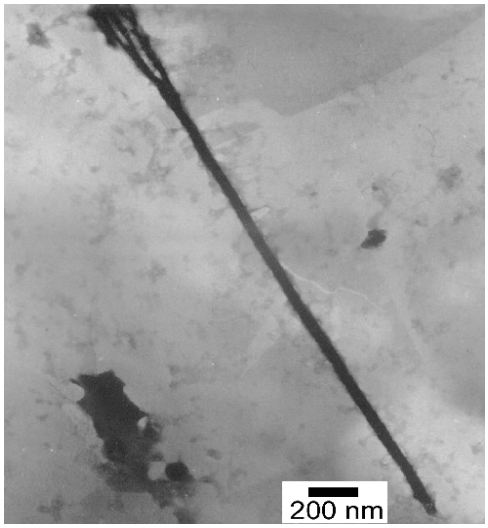

Figure 3. A TEM image of the segmented $(Ni/Fe)_2$ composite nanowires.

The dependence on the number of segments m of the coercivity H_c of the hysteresis loops obtained experimentally, with the field applied along the nanowire axis at room temperature, is shown as a dot in figure 5. It was shown experimentally that the coercivity H_c is 1423 Oe

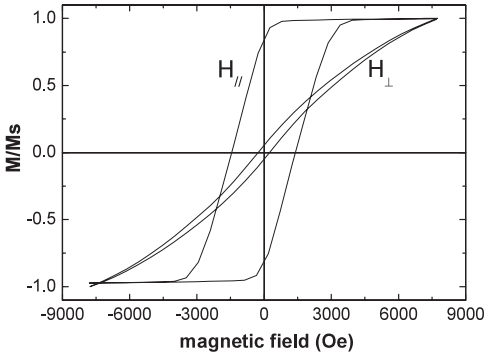

Figure 4. M–H hysteresis loops of the segmented $(Ni/Fe)_2$ composite nanowires. $H_{\parallel}$ and $H_{\perp}$ represent the applied field H being parallel and perpendicular to the wire axis.

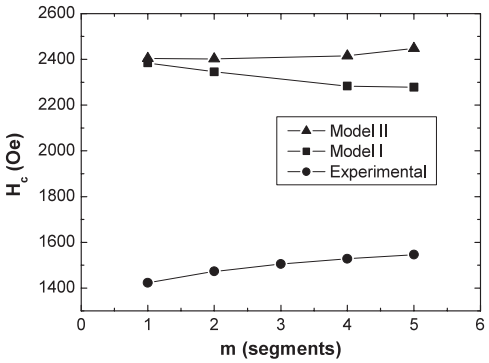

Figure 5. The dependence of H_c on the number of segments for the segmented $(Ni/Fe)_m$ composite nanowire arrays.

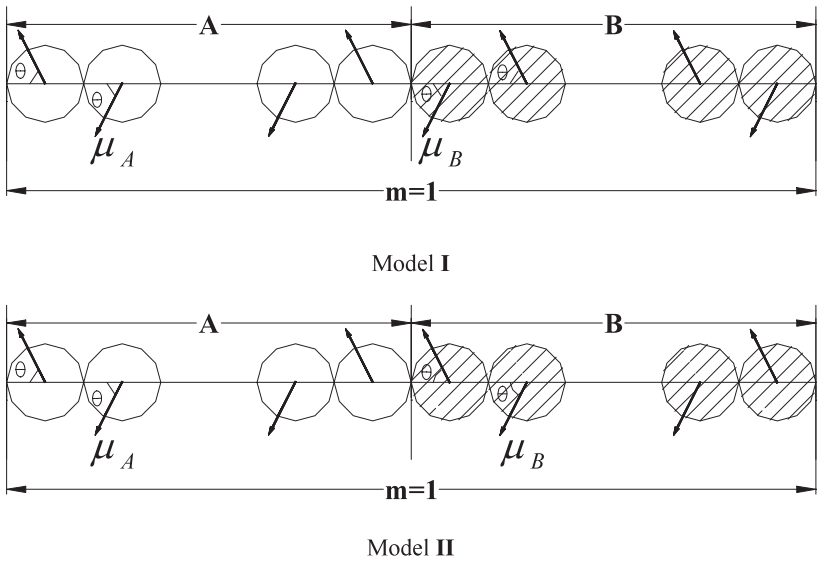

Figure 6. The chain-of-spheres model: model I—with the traditional symmetric fanning mechanism; model II—with the fanning mechanism taking into account the exchange coupling effect.

at $m = 2$, and H_c gradually increases with increasing m. However, the traditional symmetric fanning mechanism of the sphere–chain model (in model I, shown in figure 6) used to interpret the magnetization reversal process in single-metal or alloy nanowires [11, 12] gives a decreasing coercivity dependence of m, shown as a square in figure 5. It is logical to think that the exchange coupling may make an important contribution to the magnetization reversal process. In order to understand the magnetization reversal mechanism of the segmented composite nanowires, we suppose a fanning mechanism of the sphere–chain model with exchange coupling between A and B interface spheres (in model II, shown in figure 6). We suggest that, due to the effective exchange coupling between A (Fe) and B (Ni) segments, the magnetic moments of the interface Fe sphere and Ni sphere are parallel to each other, not fanning out. For model II, the coercivity

of the segmented $(\mathrm{Ni/Fe})_m$ composite nanowires can be written as

$$H_c = \frac{\pi}{6m(N_A M_{SA} + N_B M_{SB})}\Bigg[mM_{SA}^2 N_A(2L_{NA} + 6M_{NA}) + mM_{SB}^2 N_B(2L_{NB} + 6M_{NB}) + mM_{SA}M_{SB}(N_A + N_B)(2L_{AB} + 6M_{AB}) + \sum_{n=1}^{n=m-1} 2(m-n)M_{SA}^2 N_A(2L_{lm}^{AA} + 6M_{lm}^{AA}) + \sum_{n=1}^{n=m-1} 2(m-n)M_{SB}^2 N_B(2L_{lm}^{BB} + 6M_{lm}^{BB}) + \sum_{n=1}^{n=m-1} (m-n)M_{SA}M_{AB}(N_A + N_B)(2L_{lm}^{AB} + 6M_{lm}^{AB}) + \sum_{n=1}^{n=m-1} (m-n)M_{SA}M_{AB}(N_A + N_B)(2L_{lm}^{BA} + 6M_{lm}^{BA})\Bigg] \quad (1)$$

where m is the number of segments, N_A and N_B are the numbers of Fe spheres and Ni spheres, respectively (N_A and N_B are even), and M_{SA} and M_{SB} are the saturation magnetizations of Fe and Ni respectively; the sequences for numbers L and M are shown in the appendix.

As mentioned above, the deposition ratio of Fe and Ni is about 2:1 and the deposition time is the same for every segment; thus the length ratio of Fe and Ni segments is about 2:1, i.e. the number ratio of Fe spheres and Ni spheres is about 2:1. The nanowire length is about 3 μm and the diameter is about 50 nm, so the total number of Fe spheres and Ni spheres in a single nanowire is equal to the aspect ratio ($N \approx 60$). Suppose $m = 1$; then $N_A = 40$ and $N_B = 20$. If $m = 2$, then $N_A = 20$ and $N_B = 10$. The rest may be deduced by analogy. Using the above parameters, the coercivity can be calculated using equation (1). The results are also shown as the triangle in figure 5. The m dependences of the calculated results are roughly in agreement with the experimental results; at least, the rule for the coercivity variation is similar (see figure 5). Deviation from the experimental results may arise from the following factors that were neglected:

(i) The interactions between the nanowires in the AAO film: these should cause a lower coercivity in comparison with that for a single nanowire [7, 19].
(ii) The size of the particle (the diameter of the wires) is larger than the critical size of a single-domain particle.
(iii) The saturation magnetizations M_S of Fe and Ni in $(\mathrm{Ni/Fe})_m$ nanowires were assumed to be equal to those of their bulk alloys, since they could not be measured for technical reasons.
(iv) In the theoretical prediction, every experimental process was assumed to be the same.

Since the fanning mechanism of the sphere–chain model is essentially magnetostatic, it does not account for the exchange coupling between the segments. This is the reason for the disagreement between models I and II. The exchange interaction is important on an atomic scale [6, 8], so model I is unrealistic from a local point of view, but on the submicron length scale the magnetostatic interaction dominates and local features are less important.

4. Conclusions

Uniform arrays of segmented $(\mathrm{Ni/Fe})_m$ ($m = 1, 2, 3, 4, 5$) composite nanowires were fabricated by electrodeposition using a dual-bath technique. The aspect ratio is about 60.

The sets of Fe(110) and Ni(111) diffraction peaks both have preferred orientation along the wire axes and overlap. The interface spheres between Fe and Ni segments are exchange coupled, but the macroscopic behaviour can be mapped onto an effective fanning-type model (model II). It is found that the coercivity variation rule simulated by model II agrees with the experimental results.

Acknowledgments

The authors would like to express their sincere thanks to Dr J B Wang for valuable discussion. This work was supported by NSFC (Grant No 50171032) and the Trans-Century Training Programme Foundation for Talent of the MOE, People's Republic of China.

Appendix

We consider the exchange coupling of the interface spheres between the segments (model II in the figure 6), use a similar derivation of the fanning mechanism of the sphere–chain model [9], and obtain the equations (1) in the text, where L and M are as follows:

$$L_{\mathrm{NA}} = \sum_{i=1}^{N_{\mathrm{A}}-1} \sum_{j=1}^{j\leqslant\frac{N_{\mathrm{A}}+1-i}{2}} \frac{1}{N_{\mathrm{A}}(2j-1)^3} \tag{A.1}$$

$$M_{\mathrm{NA}} = \sum_{i=1}^{N_{\mathrm{A}}-2} \sum_{j=1}^{j\leqslant\frac{N_{\mathrm{A}}-i}{2}} \frac{1}{N_{\mathrm{A}}(2j)^3} \tag{A.2}$$

$$L_{\mathrm{NB}} = \sum_{i=1}^{N_{\mathrm{B}}-1} \sum_{j=1}^{j\leqslant\frac{N_{\mathrm{B}}+1-i}{2}} \frac{1}{N_{\mathrm{B}}(2j-1)^3} \tag{A.3}$$

$$M_{\mathrm{NB}} = \sum_{i=1}^{N_{\mathrm{B}}-2} \sum_{j=1}^{j\leqslant\frac{N_{\mathrm{B}}-i}{2}} \frac{1}{N_{\mathrm{B}}(2j)^3} \tag{A.4}$$

$$L_{\mathrm{AB}} = \sum_{i=1}^{i=\frac{N_{\mathrm{A}}}{2}} \sum_{j=1}^{j=\frac{N_{\mathrm{B}}}{2}} \frac{1}{N_{\mathrm{A}}+N_{\mathrm{B}}}\left[\frac{2}{(N_{\mathrm{A}}+2j-2i)^3}\right] \tag{A.5}$$

$$M_{\mathrm{AB}} = \sum_{i=1}^{i=\frac{N_{\mathrm{A}}}{2}} \sum_{j=1}^{j=\frac{N_{\mathrm{B}}}{2}} \frac{1}{N_{\mathrm{A}}+N_{\mathrm{B}}}\left[\frac{1}{(N_{\mathrm{A}}+2j-2i+1)^3}+\frac{1}{(N_{\mathrm{A}}+2j-2i-1)^3}\right] \tag{A.6}$$

$$L_{lm}^{\mathrm{AA}} = \sum_{i=1}^{i=\frac{N_{\mathrm{A}}}{2}} \sum_{j=1}^{j=\frac{N_{\mathrm{A}}}{2}} \frac{1}{N_{\mathrm{A}}+N_{\mathrm{A}}}\left[\frac{1}{[n(N_{\mathrm{A}}+N_{\mathrm{B}})+2j-2i+1]^3} + \frac{1}{[n(N_{\mathrm{A}}+N_{\mathrm{B}})+2j-2i-1]^3}\right] \tag{A.7}$$

$$M_{lm}^{\mathrm{AA}} = \sum_{i=1}^{i=\frac{N_{\mathrm{A}}}{2}} \sum_{j=1}^{j=\frac{N_{\mathrm{A}}}{2}} \frac{1}{N_{\mathrm{A}}+N_{\mathrm{A}}}\left[\frac{2}{[n(N_{\mathrm{A}}+N_{\mathrm{B}})+2j-2i]^3}\right] \tag{A.8}$$

$$L_{lm}^{\mathrm{BB}} = \sum_{i=1}^{i=\frac{N_\mathrm{B}}{2}} \sum_{j=1}^{j=\frac{N_\mathrm{B}}{2}} \frac{1}{N_\mathrm{B}+N_\mathrm{B}} \left[\frac{1}{[n(N_\mathrm{A}+N_\mathrm{B})+2j-2i+1]^3} + \frac{1}{[n(N_\mathrm{A}+N_\mathrm{B})+2j-2i-1]^3} \right] \tag{A.9}$$

$$M_{lm}^{\mathrm{BB}} = \sum_{i=1}^{i=\frac{N_\mathrm{B}}{2}} \sum_{j=1}^{j=\frac{N_\mathrm{B}}{2}} \frac{1}{N_\mathrm{B}+N_\mathrm{B}} \left[\frac{2}{[n(N_\mathrm{A}+N_\mathrm{B})+2j-2i]^3} \right] \tag{A.10}$$

$$L_{lm}^{\mathrm{AB}} = \sum_{i=1}^{i=\frac{N_\mathrm{A}}{2}} \sum_{j=1}^{j=\frac{N_\mathrm{B}}{2}} \frac{1}{N_\mathrm{A}+N_\mathrm{B}} \left[\frac{2}{[n(N_\mathrm{A}+N_\mathrm{B})+N_\mathrm{A}+2j-2i]^3} \right] \tag{A.11}$$

$$M_{lm}^{\mathrm{AB}} = \sum_{i=1}^{i=\frac{N_\mathrm{A}}{2}} \sum_{j=1}^{j=\frac{N_\mathrm{B}}{2}} \frac{1}{N_\mathrm{A}+N_\mathrm{B}} \left[\frac{1}{[n(N_\mathrm{A}+N_\mathrm{B})+N_\mathrm{A}+2j-2i+1]^3} + \frac{1}{[n(N_\mathrm{A}+N_\mathrm{B})+N_\mathrm{A}+2j-2i-1]^3} \right] \tag{A.12}$$

$$L_{lm}^{\mathrm{BA}} = \sum_{i=1}^{i=\frac{N_\mathrm{B}}{2}} \sum_{j=1}^{j=\frac{N_\mathrm{A}}{2}} \frac{1}{N_\mathrm{B}+N_\mathrm{A}} \left[\frac{2}{[n(N_\mathrm{A}+N_\mathrm{B})-N_\mathrm{A}+2j-2i]^3} \right] \tag{A.13}$$

$$M_{lm}^{\mathrm{BA}} = \sum_{i=1}^{i=\frac{N_\mathrm{B}}{2}} \sum_{j=1}^{j=\frac{N_\mathrm{A}}{2}} \frac{1}{N_\mathrm{B}+N_\mathrm{A}} \left[\frac{1}{[n(N_\mathrm{A}+N_\mathrm{B})-N_\mathrm{A}+2j-2i+1]^3} + \frac{1}{[n(N_\mathrm{A}+N_\mathrm{B})-N_\mathrm{A}+2j-2i-1]^3} \right]. \tag{A.14}$$

References

[1] Yan S S, Liu W J, Weston J L, Zangari G and Barnard J A 2001 *Phys. Rev.* B **63** 174415
[2] Zeng H, Li J, Liu J P, Wang Z L and Sun S 2002 *Nature* **420** 395
[3] Whitney T M, Jiang J S, Searson P C and Chien C L 1993 *Science* **261** 1316
[4] Zabala N, Puska M J and Nieminen R M 1998 *Phys. Rev. Lett.* **80** 3336
[5] Jorritsma J and Mydosh J A 1998 *J. Appl. Phys.* **84** 901
[6] Skomski R, Zeng H, Zheng M and Sellmyer D J 2000 *Phys. Rev.* B **62** 3900
[7] Sellmyer D J, Zheng M and Skomski R 2001 *J. Phys.: Condens. Matter* **13** R433
[8] Skomski R 2003 *J. Phys.: Condens. Matter* **15** R841
[9] Jacobs I S and Bean C P 1955 *Phys. Rev.* **100** 1060
[10] Jacobs I S and Luborsky F E 1957 *J. Appl. Phys.* **28** 467
[11] Almawlawai D, Coombs N and Moskovits M 1991 *J. Appl. Phys.* **70** 4421
[12] Zhan Q F, Chen Z Y, Xue D S and Li F S 2002 *Phys. Rev.* B **66** 134436
[13] Jessensky O, Müller F and Gösele U 1998 *Appl. Phys. Lett.* **72** 1173
[14] Strijkers G J, Dalderop J H J, Broeksteeg M A A, Swagten H J M and de Jonge W J M 1999 *J. Appl. Phys.* **86** 5141
[15] Nielsch K, Wehrspohn R B, Barthel J, Kirschner J and Gösele U 2001 *Appl. Phys. Lett.* **79** 1360
[16] Blondel A, Doudin B and Ansermet J-Ph 1997 *J. Magn. Magn. Mater.* **165** 34
[17] Goldman L M, Ross C A, Ohashi W, Wu D and Spaepen F 1989 *Appl. Phys. Lett.* **55** 2182
[18] Masuda H and Fukuda K 1995 *Science* **268** 1466
[19] Garcia J M, Asenjo A, Velazquez J, Garcia D, Vazquez M, Aranda P and Ruiz-Hitzky E 1999 *J. Appl. Phys.* **85** 5480